Structure and Stability of Modern Electrolytes in Nanoscale Confinements from Molecular Dynamics Perspective

Harender S. Dhattarwal and Hemant K. Kashyap

Abstract Recent studies show that ionic liquids and high concentration salt solutions are promising alternatives to conventional electrolytes for high-performance batteries. The intercalation of electrolytes in nanoscale electrode confinements is a vital phenomenon governing the performance of batteries. A fundamental understanding of the electrolyte structure and stability inside electrode confinements helps explore the full potential of modern electrolytes for electrochemical devices. Factors such as the confinement shape, size, and flexibility govern the stability of electrolytes in nanoscale confinements. Enhanced molecular dynamics simulation can help delineate the free energy underlying the process of electrolyte evaporation or deintercalation from confinements. However, such studies in this direction are limited to few electrolytes only. This chapter highlights recent computational studies carried out in our group exploring the stability and structure of ionic liquids and water-in-salt electrolytes in nanoscale confinements, and provides a plausible mechanism for their intercalation and deintercalation behaviour.

Keywords Electrolytes · Intercalation · Water-in-salt · Ionic liquids · Umbrella sampling · Molecular dynamics

1 Introduction

The field of energy storage has been dominated by lithium ion batteries (LIBs) for the past few decades [1–3]. Electrolytes in conventional energy storage devices usually contain Li salt with volatile and flammable organic solvents, resulting in safety concerns while operating at higher temperatures and larger scale [1, 3–6]. The demand for clean and sustainable electrolytes is increasing for their use in energy

H. S. Dhattarwal · H. K. Kashyap (✉)
Department of Chemistry, Indian Institute of Technology Delhi, Hauz Khas, New Delhi 110016, India
e-mail: hkashyap@chemistry.iitd.ac.in
URL: https://web.iitd.ac.in/ hkashyap/

I. Uddin and I. Ahmad (eds.), *Synthesis and Applications of Nanomaterials and Nanocomposites*, Composites Science and Technology ,
https://doi.org/10.1007/978-981-99-1350-3_5

storage applications in electric vehicles and grid storage. Ionic liquids (ILs) and highlyconcentrated water-in-salt (WIS) electrolytes show great potential to replace conventional electrolytes in next-generation high-capacity batteries [7–9]. ILs are complex salts that are liquid below 100 °C and do not contain any neutral molecular species such as water or organic solvents [10]. ILs exhibit unique properties such as a wide electrochemical window, nonvolatility, high chemical and thermal stability, and high ionic conductivity, which make them suitable candidate for energy storage [11–20]. Several studies have demonstrated the capability of ILs to improve the performance of supercapacitors [21–26]. WIS electrolytes are another class of electrolytes that have emerged as novel electrolytes for high performance batteries. WIS electrolytes have a salt to solvent ratio greater than 1, i.e., they have more amount of salt than water in mass and volume [9]. WIS electrolytes belong to a wider range of "solvent-in-salt" electrolytes which are also termed as highly concentrated electrolytes [27]. These electrolytes consist of large amount of salts dissolved in different solvents [28–30]. Like ILs, WIS electrolytes also possess enhanced redox stability and a wide electrochemical window [9, 29, 31–34]. Highly concentrated or superconcentrated solutions have been frequently explored as electrolytes in batteries [27, 30, 32, 35–38].

In an electrochemical system, electron transfer occurs at the electrode-electrolyte interface. The distribution of electrolyte species at the interface governs the interfacial reactions occurring within the electrochemical devices. Understanding the structure and distribution of the electrolytes at the model electrode surfaces helps determine their capability to be used in batteries and capacitors [39]. Many studies on the nanodroplets of ILs on electrode surface have revealed that the structure of ionic liquids at the interface and the extent of wetting are dependent on the extent of hydrophobic or hydrophilic nature of the surface [40–48]. The structure of ILs has been studied extensively near different electrode surfaces at varying potentials [49–54]. Similar but limited number of studies are also available on the WIS electrolytes under confinement or on electrode surfaces [55–57]. However, most simulation studies explored the electrodes having smooth surfaces and only the van der Waal and electrostatic interactions between the electrode and electrolyte molecules have been considered. Although, the findings in the above mentioned endeavours were very insightful, an ideal electrode in energy storage devices possesses rough surfaces with pores of different shapes and sizes [58–60]. The actual performance of the device also depends on the wetting of these nanopores by the electrolyte molecules or ions. Additionally, in LIBs the process of charging and discharging involve intercalation and deintercalation of electrolyte species at the anode and cathode [3, 61]. The computational studies focusing on the structure of the electrolytes in the nanoscopic confinements and intercalation of electrolytes in electrodes are scarce in the literature. In this chapter, we made an effort to compile our recent studies on the structure and thermodynamics stability of confined ILs and WIS electrolytes using molecular simulations.

The interaction of a solvent/solution confined between sufficiently separated hydrophobic sheets induces the transition from liquid to vapor phase (or evaporation) inside the nanoscale confinement (capillary). The process of capillary evaporation of water from solvophobic confinements has been explored through number of theoretical and computer simulations studies [62–66]. Huang et al. showed that water can evaporate from a hydrophobic confinement when the separation between two confining plates is less than a critical separation d_c. Also, the vapor phase of water inside the confinement stays in vapor phase below d_c. However, near the d_c, the liquid and vapor phases of water are found to be in equilibrium [62]. Remsing et al. showed that the process of capillary evaporation of water from solvophobic confinement starts as vapor bubble nucleation on the confining surface. The vapor bubble then spans across the confinement to form a vapor tube, which further grows in size, leading to transition from liquid phase to vapor phase of water between the confining plates [64]. Altabet et al. further verified the vapor tube formation as a critical point in the process of water evaporation and showed that the process is significantly affected by the confinement flexibility [65]. Davoodabadi and Ghasemi have recently summarized the studies on the evaporation of water from nanoscale confinements [67]. The literature on the structure and thermodynamics of water inside different confinements is very extensive. However, number of such studies on ILs or WIS electrolytes is limited. Similar to capillary evaporation, the movement of electrolyte species in (intercalation) and out (deintercalation) of electrode vacant sites is also influenced by the electrode properties [61, 68–73]. The deintercalation of electrolytes from the electrode can be modelled by mimicking the process of capillary evaporation of water from solvophobic confinements [74–76].

In this chapter, we have reviewed the work done by our group on the stability of electrolytes in nanoscale carbon confinements. In the following sections, we highlight different key factors that govern the process of electrolyte intercalation/deintercalation and their stability inside solvophobic nanopores. Finally, the structure of electrolyte between the confining sheets is discussed. We limit the discussion in this chapter to the computer simulation studies of ionic liquids and water-in-salt electrolytes in nanoscopic graphene/graphite like hydrophobic confinements.

2 Stability of Electrolytes

Stability of electrolytes in confinement is usually discussed in terms of their phase behavior. When the electrolyte is stable inside the confinement, it usually tends to be in condensed phase, i.e., the density and structure of the electrolyte inside the confinement is comparable to that in the bulk [76]. However, when the electrolyte is unstable between the confining surfaces, it usually exists in vapor phase or does not prefer to stay in the confinement at all. In this case, the density of electrolyte within the confining region is significantly lower than the bulk density.

2.1 Process of Deintercalation

The process of change of electrolyte phase from its liquid to vapor phase inside a confinement is called deintercalation of the electrolyte, or sometimes termed as capillary evaporation [66, 76, 77]. The mechanism and thermodynamics of electrolyte intercalation-deintercalation have been studied by modelling electrolyte inside nanoscale confinement created by two parallel flat surfaces separated by a distance d [75, 76]. The interaction between the electrolyte and the confining sheets can be tuned by tweaking the parameters of the corresponding potential energy functions. The confining surfaces is considered solvophobic when the strength of the interaction, usually defined through the Lennard-Jones potential of the surface atoms, is weak and the contact angle formed by the electrolyte is more than 90° [48]. For example, the contact angles formed by 1-ethyl-3-methylimidazolium tetrafluoroborate ([EMIM][BF_4]) ionic liquid and Li bis(trifluoromethane)sulfonimide ([Li][TFSI]) WIS electrolyte on the model surfaces discussed here are around 140° and 130°, respectively [74, 76].

The electrolyte density fluctuations inside the confinement are probed using the indirect umbrella sampling (INDUS) technique [78, 79]. The free energy of electrolyte phase transition inside the confinement is estimated through probability ($P_v(N)$) of finding the N atoms or species of the electrolyte between the confining surfaces, separated by a distance d, with a confinement volume v. Shrivastav et al. used total number of heavy atoms of the ions of [EMIM][BF_4]as the order parameter of enhanced sampling whereas Dhattarwal et al. probed total number of atoms or species of [Li][TFSI] WIS electrolyte inside the confinement as the order parameter [74, 75]. A harmonic biasing potential is applied to maintain number of species inside the confinement to the target value N^* which typically varies in the range from vapor phase to liquid phase,

$$U(\widetilde{N}) = \frac{\kappa}{2}(\widetilde{N} - \widetilde{N}^*)^2. \tag{1}$$

Here, the biasing potential is applied on the continuous and coarse-grained variant of order parameter, $\widetilde{N}$ [78, 79]. κ is the spring force constant which guarantees the sampling of the phase space close to the target value of the order parameter. Figure 1 represents the simulation snapshots of a WIS electrolyte inside the nanoscale solvophobic sheets depicting a phase transition from vapor phase (VP) to liquid phase (LP). The free energy of phase transition is estimated from the probability distribution obtained from the enhanced sampling simulations using the weighted histogram analysis method (WHAM) as:

$$\Delta \mathrm{G}(N) = -\beta^{-1} \ln P_v(N), \tag{2}$$

where $\Delta \mathrm{G}(N)$ is free energy of the phase corresponding to N species inside the confinement, $\beta = 1/k_B T$, and T and k_B are the temperature and the Boltzmann's

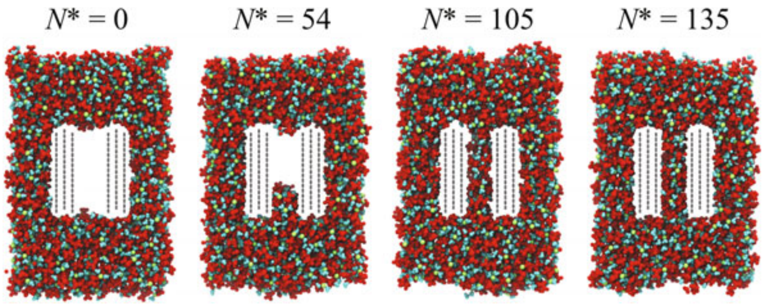

Fig. 1 Simulation snapshots of [Li][TFSI] based WIS electrolyte inside nanoscale solvophobic confinements for different number of target species between the confining sheets illustrating the transition between vapor and liquid phases of the electrolyte. The confining solvophobic carbon sheets are separated by 1.5 nm. Green, red, cyan, and grey beads represent $[Li]^+$, $[TFSI]^-$, water molecules, and carbon atoms of the sheets, respectively

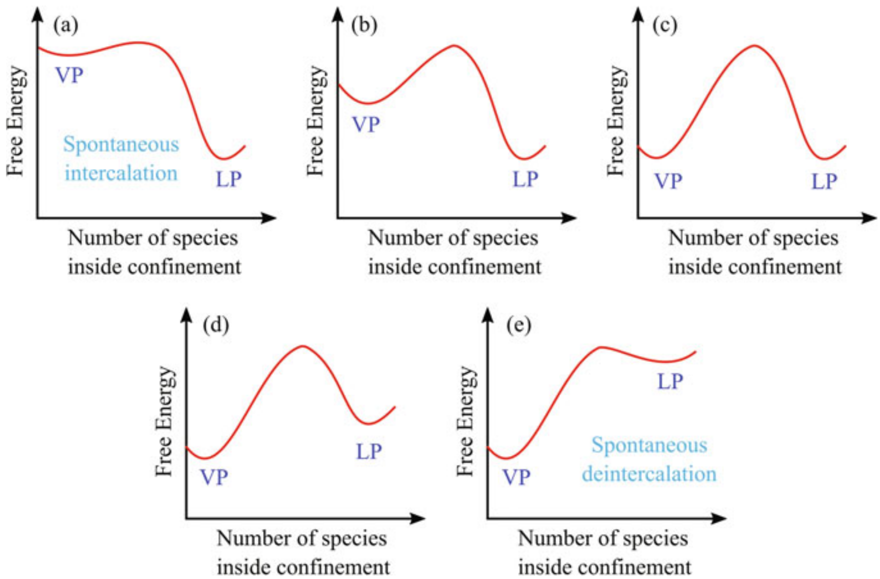

Fig. 2 Schematic illustration of different possible free energy profiles and stability of liquid/condensed (LP) and vapor phase (VP) of an electrolyte inside nanoscale confinements

constant, respectively [80]. The studies reviewed in this chapter discuss the simulations performed at 310 K temperature.

The relative stability of liquid and vapor phases, and the process of electrolyte deintercalation from a nanoscale solvophobic or ionophobic confinement can be described in five different scenarios summarized through the illustration shown in Fig. 2.

(a) In the first case, the free energy of LP is significantly lower than the VP, and there is no well-defined VP (see Fig. 2a). In this case, only the LP is stable inside the confinement and intercalation of electrolyte into the confinement is spontaneous.
(b) In the second case, the free energy of LP is lower than that of VP and both the phases are separated by a appreciable free energy barrier. In this case, the LP is stable inside the confinement and VP is metastable (see Fig. 2b). Here, the LP is more favourable inside the confinement, however, VP requires some amount of energy in order to make transition to LP or vice versa.
(c) In the third case, both VP and LP have same free energy but are separated by a significant free energy barrier (see Fig. 2c). Here, both the phases are stable inside the confinement and phase transition between them is energy intensive in both directions.
(d) In the fourth case, free energy of VP is lower than the LP and a free energy barrier separates both the phases. Here, the VP is more stable inside the confinement than the LP, which is metastable (see Fig. 2d). However, the free energy barrier needs to be crossed for the transition from LP to VP or vice versa.
(e) In the fifth case, the free energy of VP is significantly lower than the LP and there is no free energy barrier for LP to VP transition (see Fig. 2e). Here the process of deintercalation of the liquid or electrolyte is spontaneous, and their constituent species do not stay in the confinement.

There are multiple factors that govern the relative stability of vapor and liquid phases of electrolytes inside the confinement. In the following sections, we have discussed recent studies exploring the effect of these factors on the process of intercalation and deintercalation of electrolyte species.

2.2 Dependence on the Surface Area and Separation of Confining Sheets

Along with the surface area, the separation between the nanoscale sheets confining the electrolyte is one of the major factors that governs the relative stability of liquid and vapor states of electrolytes inside the confinement [74–76].

Figure 3 shows the simulated free energy plotted as a function of number (N) of [EMIM][BF_4] heavy atoms inside the solvophobic carbon confinements at different interplate separations [74]. Here, all the free energy profiles are shifted such that the free energy of the LP of [EMIM][BF_4] is at zero. Basins or minima with smaller N values on the x-axis correspond to VP of [EMIM][BF_4] inside the confinement. Similarly, the basins formed at larger N values correspond to the LP of [EMIM][BF_4]. The free energy profiles have a parabolic distribution at the LP basins, which deviates to a fat tail as the N value decreases (see inset of Fig. 3). At the larger d values, e.g. 1.6 nm, there is no well-defined basin for the VP, and the LP is the only stable state of [EMIM][BF_4] inside the confinement. As the inter-plate separation is decreased

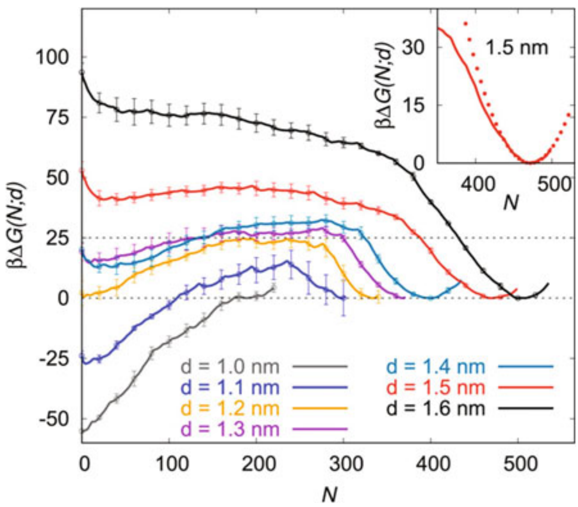

Fig. 3 Simulated free energy profiles showing variation in the free energy ($\beta\Delta G(N; d)$) for [EMIM][BF_4] as a function of number of heavy atoms inside the solvophobic confinements at different separations. Inset highlights that in the region corresponding to the condensed or liquid phase of [EMIM][BF_4] (higher N values), the free energy profiles follow a inverted Gaussian or parabolic distribution, and deviations from the inverted Gaussian distribution are observed while moving towards the vapor phase region. Reprinted with permission from Ref. [74], Copyright 2018 AIP

to 1.5 nm, a minimum corresponding to the VP starts to emerges in the smaller N region of the free energy profile.

However, the free energy of this basin is still more than the LP basin, and the VP is metastable. With further decrease in the inter-plate separation, the free energy of vapor basin decreases. When the inter-plate separation is 1.2 nm, the free energy of vapor and liquid phases is same, reflecting that both the states are stable at this separation. However, the free energy barrier separating the two states is significantly high. The separation at which the LP and VP are having same free energy is called as critical separation, d_c [62]. At this separation, the free energy cost of phase transition between vapor and liquid phases is very high. Moreover, below the critical separation, the VP tends to be more stable and LP become metastable. If the interplate separation is further decreased, the energy barrier between the liquid and vapor phases significantly decreases and the free energy cost for the liquid to vapor phase transition decreases. Below or at 1 nm separation between the confining surfaces, the free energy barrier vanishes, and the transition from LP to VP becomes a spontaneous process.

The dependence of stability of WIS electrolyte on the separation between confinement sheets is similar to ILs and water [76]. Figure 4 shows the simulated free energy plotted as a function of number of WIS species inside the solvophobic carbon confinements at different interplate separations. The figure reveals that the electrolyte is

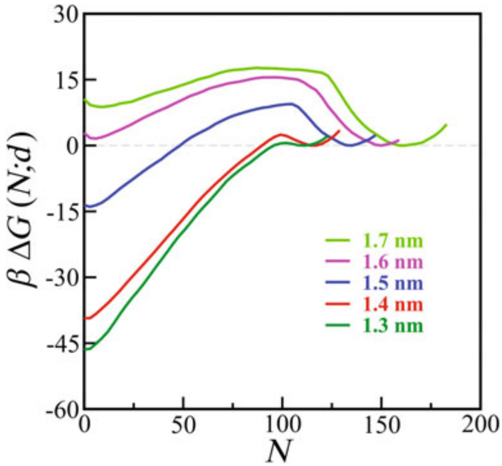

Fig. 4 Simulated free energy profiles ($\beta\Delta G(N; d)$) for [Li][TFSI]/water WIS electrolyte as a function of number of electrolyte species inside the solvophobic confinements at different separations. The height of the barrier separating the liquid and vapor phases of the WIS electrolyte within the confinement decreases with decrease in the separation between the confining surfaces. Reprinted with permission from Ref. [76], Copyright 2021 RSC

more stable inside nanoscale confinements at higher interplate separations, and at significantly lower separation, deintercalation of electrolyte is spontaneous. However, the critical separation, d_c, at which the liquid and vapor phases are equally stable is at around 1.6 nm, as compared to 1.2 nm in case of [EMIM][BF_4][74]. Similarly, the spontaneous evaporation of electrolyte from the confinement is observed at around 1.3 nm, which is significantly higher than 1 nm observed in case of [EMIM][BF_4]. These observations show that although with an increase in the confinement separation, the height of the free energy barrier separating the liquid and vapor phases increases for different electrolytes and water, the extent by which the barrier height increases depends on the type of electrolyte.

2.3 Dependence on the Confinement Flexibility

Most simulation studies on confined electrolytes have considered rigid sheets to model the confinement, by freezing the motion of their atoms. However, significant effect of confinement flexibility has been shown on the stability of VP and LP of water as well as ILs between solvophobic sheets [65, 75]. Figure 5 shows the simulated free energy profiles as function of number of [EMIM][BF_4] species inside rigid and flexible solvophobic carbon confinements at three different interplate separations. At all the three separations, introduction of flexibility resulted in slight broadening of the liquid basin. The effect of confinement flexibility is more prominent on the

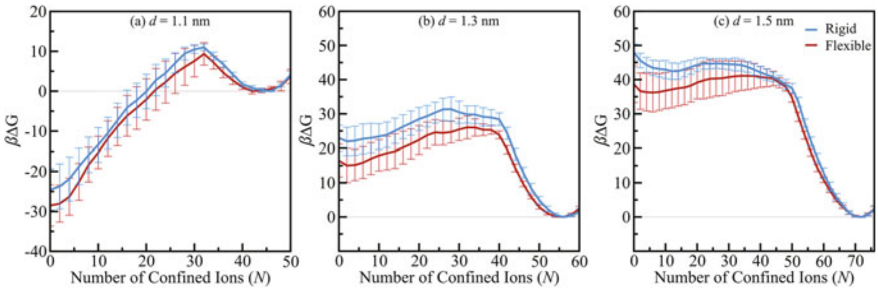

Fig. 5 Comparison between the simulated free energy profiles ($\beta\Delta G(N; d)$) for [EMIM][BF_4] as a function of number of ions inside the rigid (blue) and flexible (red) solvophobic confinements at three different separations. At all the three interplate separations studied, the free energy of [EMIM][BF_4] deintercalation from the flexible confinements is lower than the rigid confinements. Reprinted with permission from Ref. [75], Copyright 2020 ACS

vapor basin. The stability of vapor phase of [EMIM][BF_4] is significantly increased between the flexible solvophobic carbon sheets. Theoretical predictions attribute this enhanced stability to decrease in effective volume inside the confinement at lower N values [81]. When the electrolyte is in VP, a pressure difference builds up at the confinement sheets due to low density of electrolyte inside the confinement and high density of electrolyte outside the confinement. This pressure difference along with the interfacial tension in the flexible sheets lead to surface deformations, resulting in lowered confining volume [75, 81]. However, the effect of the pressure difference on the sheets is negligibly small when the electrolyte inside the confinement is in liquid state, hence, the stability of liquid state of electrolyte is not affected much by the confinement flexibility.

2.4 Dependence on the Electrolyte Concentration

Along with confinement characteristics like separation, size, and flexibility, salt concentration also governs the deintercalation process in WIS electrolytes. Figure 6 shows the free energy profiles for the WIS electrolyte as a function of number of species inside the confinement at three different concentrations for a fixed interplate separation of 1.7 nm. For 20 m (molal) salt solution, the LP of the electrolyte is more stable and VP is metastable inside the confinement. However, when the concentration is lowered to 10 m, the VP becomes more stable and LP is metastable. Just like critical separation, there is a critical concentration at which the liquid and vapor phases have similar free energies. For [Li][TFSI]-water system, the critical concentration lies between 10–20 m. With further lowering the concentration to 5 m, the VP is even more stable and the free energy barrier of liquid to vapor transition is lowered. It is expected that at even lower concentrations of the salt, the free energy barrier would further decrease and the process of electrolyte deintercalation will be spontaneous.

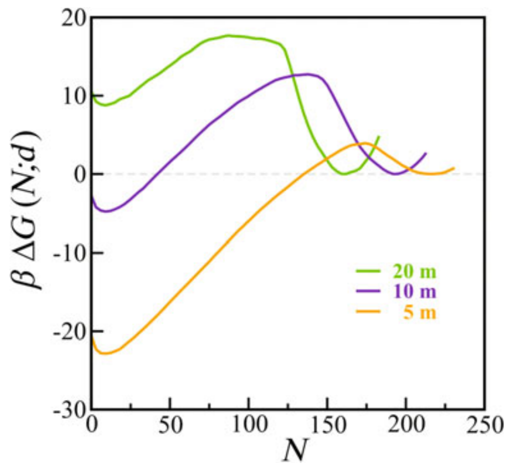

Fig. 6 Simulated free energy profiles ($\beta\Delta G(N;d)$) for three different concentration of [Li][TFSI]-water WIS electrolyte as a function of number of electrolyte species inside the solvophobic confinements at an interplate separation of 1.7 nm. Lowering the concentration of [Li][TFSI] in water resulted in significant increase in the stability of VP of electrolyte inside the confinement. Reprinted with permission from Ref. [76], Copyright 2021 RSC

3 Mechanism of Electrolyte Deintercalation

The mechanism of capillary evaporation or deintercalation of water from nanoscale solvophobic confinements involves the formation of a vapor bubble on the surface of the confinement that further grows to complete removal of water from the confinement [64, 65]. Similarly, the mechanism of deintercalation of WIS electrolyte was predicted by studying the growth of vapor bubble inside solvophobic confinement. Figure 7 shows the vapor bubble formed between the carbon surfaces (d = 1.5 nm), represented by the interface formed by the liquid (or solution) and vapor phases. When the electrolyte inside the confinement is in LP, there is no vapor bubble between the surfaces. As the number of species inside the confinement decreases, the vapor bubbles begin to appear on the opposite sides of the confinement. At an interplate separation of 1.5 nm, this process of vapor bubble formation is energy intensive. Decreasing the number of species inside the confinement requires further energy cost which leads to a gap-spanning vapor bubble formation across the confining sheets. The vapor bubble then further grows in size to eventually cover up the whole space between the surfaces, and the electrolyte is completely deintercalated from the confinement.

The process of vapor bubble formation starting from the LP follows a linear equation and growth of vapor tube can be described using macroscopic theory, [64, 76] i.e., $\Delta G_{\mathrm{p}}(r; d) = \Delta G_{\mathrm{th}}(r; d) - 2k_{\mathrm{B}}T \ln(1 - 2r/L)$, where r is the radius of vapor tube forming inside the confinement, $L = 3$ nm is the side length of the confining surface, and the translational entropy of the tube is represented by the logarithmic

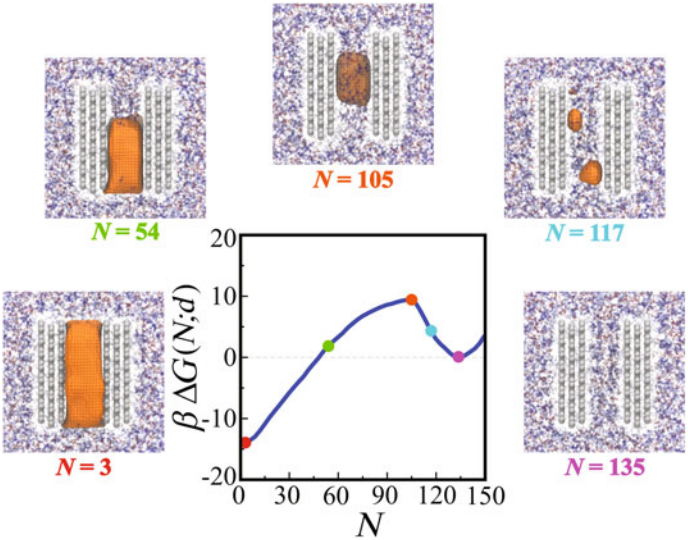

Fig. 7 Illustration of liquid-vapor interface formed inside the solvophobic carbon confinements rendered at different points along the free energy profile. Here, the concentration of the salt in the WIS electrolyte is 20 m and the separation between confining sheets is 1.5 nm. $N = 135$ corresponds to LP of WIS electrolyte, at $N = 117$ vapor bubbles begin to form, at $N = 105$ the bubbles join to form gap-spanning vapor tube, and $N = 54$ to $N = 3$ represent the growth of vapor tube inside the confinement. Reprinted with permission from Ref. [76], Copyright 2021 RSC

term. Also,

$$\Delta G_{\text{th}}(r; d) = 2\pi \gamma_{vl} \left[r^2 \cos\theta + r \left(\tilde{d} + \frac{2\lambda}{\gamma_{vl}} \right) \right], \tag{3}$$

where γ_{vl} and λ are the surface and line tensions obtained from the fitting of free energy profiles, respectively. Figure 8 shows the simulated free energy profiles for the process of electrolyte deintercalation from the confinement of nanoscale sheets at three different separations and two different concentrations of electrolyte. The free energy corresponding to the process of vapor bubble formation is fitted using linear equation and the growth of gap-spanning vapor tube is fitted using macroscopic theory [76]. For WIS system at smaller d value (1.4 nm), single free energy fitting is sufficient to describe the growth of vapor tube inside the confinement (see Fig. 8a). At this separation, the vapor tube once formed between the confining sheets is already of supercritical size and requires no further energy for complete deintercalation of electrolyte. Remsing et al. reported a similar kind of supercritical point in the capillary evaporation of water from solvophobic nanoscale carbon confinements [64]. However, at larger interplate separations ($d = 1.6$ and 1.7 nm) the free energy of vapor tube growth is best described by two separate fits. At larger d values, the vapor tube initially formed between the sheets is of subcritical size and requires more energy to reach the supercritical point after which the deintercalation of electrolyte

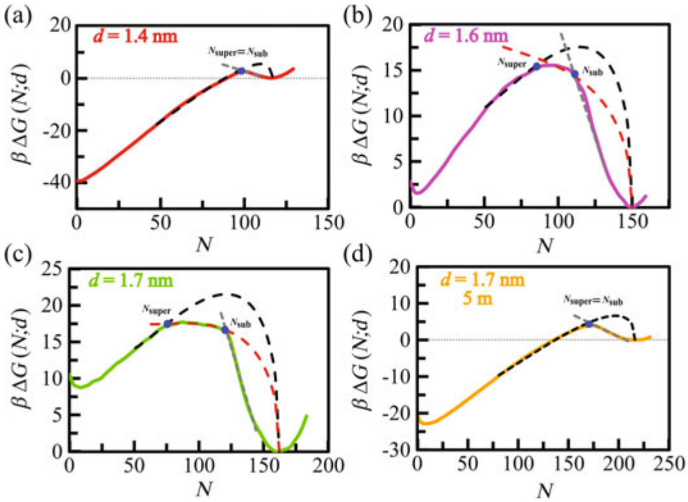

Fig. 8 The free energy profiles ($\beta\Delta G(N; d)$) for (**a**–**c**) 20 m and (**d**) 5 m concentration of WIS electrolyte inside carbon confinements as function of number of electrolyte species between the confining sheets. These profiles are fitted for different processes of electrolyte deintercalation using macroscopic theory as per Eq. 3. Grey dashed lines represent the formation of vapor bubble inside the confinement, red dashed lines represent the growth of subcritical vapor tube to its supercritical size, and black dashed lines represent the growth of supercritical vapor tube to vapor phase of the electrolyte. Reprinted with permission from Ref. [76], Copyright 2021 RSC

is spontaneous. Based on this analysis, Dhattarwal et al. described the electrolyte deintercalation from solvophobic confinements as a three step process [76].

1. The deintercalation is initiated by the formation of vapor bubbles on the opposite walls of the confinement surface. These vapor bubbles then join to form a gap-spanning vapor tube.
2. At the larger separations, the vapor tube formed is of subcritical size and grows further in size to reach at the supercritical size via an energy intensive process.
3. Once the vapor tube attain supercritical size, its size spontaneously increases, resulting in complete deintercalation of the electrolyte from the confinement.

4 Structure of Electrolytes Within the Confinement

Recent studies have highlighted the importance of local density fluctuations in governing the stability of water and electrolytes inside the nanoscale hydrophobic confinements [65, 75, 76]. The confining surface area and intersurface separation have been found to influence the distribution of electrolyte species within the confinement. The structural features of electrolytes between the confining sheets are usually stud-

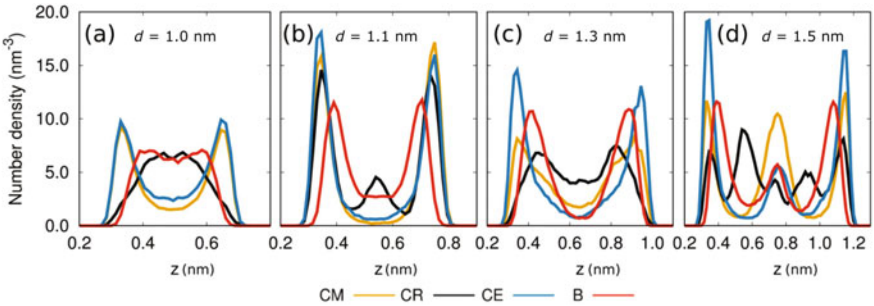

Fig. 9 Number density profiles corresponding to the terminal methyl and ethyl carbons (CM and CE) and ring carbon (CR) of $[EMIM]^+$ and boron atom (B) of $[BF_4]^-$. The profiles show highly structured and layered distribution of IL species inside the microscopic confinements. Reprinted with permission from Ref. [74], Copyright 2018 AIP

ied through number density distributions of the constituent species corresponding to the LP of confined electrolyte [74, 82].

Figure 9 depicts the number density distribution of terminal (CM and CE) and ring carbon (CR) of $[EMIM]^+$ cation and the boron atom (B) of $[BF_4]^-$ anion between two solvophobic carbon sheets at different separations [74]. Figure 9 shows the $[EMIM][BF_4]$ species inside the confinement are highly structured. At small separation (d = 1.0 nm), the non-overlapping peaks corresponding to ring and terminal carbons suggest that the cations inside the confinement are distributed in a single layer and are perpendicular to the surface of the confining sheets. Note that the end-to-end expansion of $[EMIM]^+$ and $[BF_4]^-$ along the longest axis is around 0.75 nm and 0.19 nm, respectively. At interplate separation of 1.1 nm, the peaks for the terminal carbons (methyl and ethyl ends of $[EMIM]^+$) and ring carbon overlap near the confinement surface, suggesting two parallel layers of the ions. However, few cations also attain perpendicular orientation as reflected by the central peak for CR. At d = 1.3 nm, again two layers of the ions are present, however, their orientation is not parallel to the surface of the sheets. For intersurface separation of 1.5 nm, there are five peaks corresponding to the cation ring carbon. Three of these peaks overlap with the terminal carbon near the surface and at the center of the confinement, reflecting three layer distribution of the cation in parallel orientation. Some cations also attain orientations perpendicular to the confining surfaces between the parallel layers. Dhattarwal et al. also reported the layered distribution of $[EMIM][BF_4]$ inside the nanoscale confinement and confirmed the orientational preferences of ions at different separations using orientational order parameter.

Similar to $[EMIM][BF_4]$, highly structured distribution of electrolyte species inside nanoscale solvophobic confinement was observed in case of WIS solutions [75]. Figure 10 depicts the distribution of species of [Li][TFSI]-water electrolyte within the solvophobic confinement. Note that the end-to-end expansion of $[TFSI]^-$ along the longest axis is around 0.76 nm. At lower intersurface separation (d = 1.3 nm), the [TFSI]- anions prefer to align perpendicular to the confinement surface

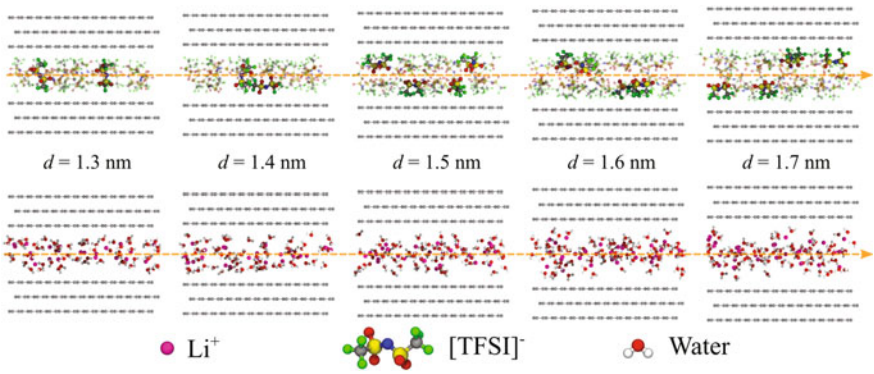

Fig. 10 Simulation snapshots representing the distribution of WIS electrolyte species between the solvophobic carbon sheets. The upper row shows the distribution of $[Li]^+$ and $[TFSI]^-$ ions, whereas, the lower row represents the distribution of water molecules inside the confinement. Magenta, blue, green, red, yellow, and white beads represent the lithium, nitrogen, fluorine, oxygen, sulphur, and hydrogen atoms, respectively. Reprinted with permission from Ref. [76], Copyright 2021 RSC

and water molecules are distributed throughout the confinement. As the separation between the sheets increases, some of the anions prefer to align parallel to the surface. Even at higher separations, most anions prefer parallel orientation and the separation between two parallel layers of anions increases with increase in interplate separation. The additional space results in more water molecules inside the confinement at higher separations, which is also reflected in the number density profiles. This also results in lower anion to water ratio between the confinement at higher interplate separations. It has also been shown that at the supercritical point, the height of the free energy barrier separating liquid and vapor phases of the electrolyte is directly correlated with the amount of salt ion pairs present within the confinement when the electrolyte is in the liquid phase [76].

5 Structural Changes During Electrolyte Deintercalation

In the previous section, we observed that the electrolytes within the nanoscale confinements are highly structured in their liquid phases. In this section, we shall examine the changes in the structure and orientation of electrolyte species during the process of electrolyte deintercalation (capillary evaporation). Figure 11 shows the joint density distribution ($\rho(z, \theta)$), which represents the number density of $[EMIM]^+$ ring vectors between the rigid and flexible confining sheets along z direction forming an angle θ with the axis perpendicular to confinement surfaces. When $[EMIM][BF_4]$ inside the confinement is in LP ($N^* = 56$), the cations prefer to align parallely near the surface ($\theta = 90°$) and perpendicularly at the center of the confinement ($\theta = 180°$). The plots

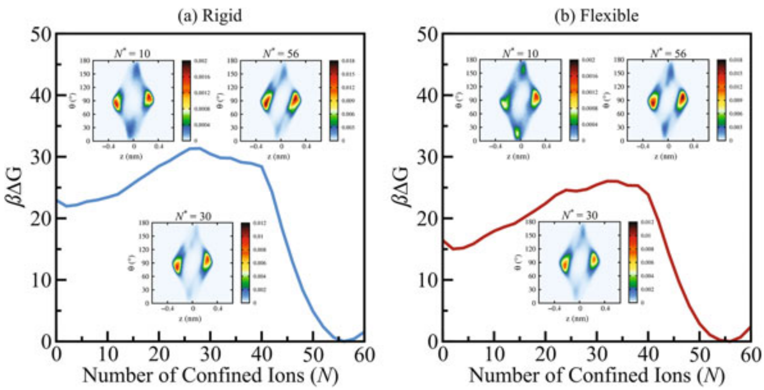

Fig. 11 The joint density distribution, $\rho(z, \theta)$, plotted along the free energy profile for [EMIM][BF_4] representing the changes in orientation of $[EMIM]^+$ ions during the deintercalation (high to low N values) of electrolyte from the solvophobic confinement. Reprinted with permission from Ref. [75], Copyright 2020 ACS

show that for flexible sheets the number density of perpendicular cations at the center of the confinement are relatively higher. As the number of [EMIM][BF_4] species inside the confinement is decreased ($N^* = 30$), the enhanced preference of perpendicular cations between flexible sheets facilitates the formation of vapor tube at the confinement surface. The difference in the preference of perpendicular orientation of cations is more prominent when the [EMIM][BF_4] reaches towards the vapor region ($N^* = 10$). Here, the ease of vapor tube formation between flexible sheets results in lower energy barrier and relatively more stable vapor phase of [EMIM][BF_4].

6 Summary and Future Directions

This chapter was focused on highlighting the recent advances in computer simulation studies on understanding the effect of confinement size, separation, flexibility, and electrolyte concentration on the process of intercalation-deintercalation of ions of neoteric electrolytes, such as ILs and WIS electrolytes, through nanoscopic confinements. These studies have clearly demonstrated that the stability of VP and LP of an IL or WIS electrolyte inside a hydrophobic confinement depends on the distance between the confining sheets. In the case of WIS electrolyte, stabilization of VP and LP also depends on the concentration of the salt. In LP, the structure of the electrolytes inside the confinement can be distinct from the bulk depending the interplate separation. It has also been demonstrated that above a critical separation between the sheets, LP is more stable for a given concentration of electrolyte. Similarly, for a given separation between the confining sheets, there exists a critical concentration of electrolyte above which the LP of the electrolyte is stable inside the confinement.

Additionally, introducing flexibility to the confining sheets decreases the free energy barrier of transition from LP to VP of the confined electrolyte.

Similar to the process of capillary evaporation of water from a hydrophobic nanoscale confinements, the deintercalation of electrolytes also starts with a vapor bubble formation at the confinement surface. Then the vapor bubble grows to form a gap-spanning vapor tube, which eventually covers the whole confinement. However, contrary to water, the size of vapor tube formed is supercritical in case of WIS electrolytes only at lower interplate separations. At higher separations, deintercalation of electrolyte is a four step process; formation of vapor bubble(s), formation of subcritical vapor tube, growth of vapor tube to supercritical size, and further spontaneous growth of vapor tube. It is evident that because of their unique nature, ILs and WIS electrolytes can be tailored to achieve higher extent of intercalation.

The distribution of ILs and WIS electrolytes within the microscopic confinements were found to be highly structured in their liquid phases. The structure of electrolyte between the confining sheets plays an important role in governing the process of electrolyte intercalation and deintercalation. Preferential deintercalation (dewetting) of ILs from flexible surfaces makes the process of electrolyte deintercalation more feasible from flexible confinements.

Although we have discussed some detailed studies on the stability of modern electrolytes inside nanoscale confinements but there are few important aspects that still remain unaddressed. Work needs to be done with a wider range of electrolytes along with utilization of confinement materials other than graphene or graphite. Effect of surface charge or potential on the stability of electrolytes inside microscopic confinements is also not fully understood. We believe that future studies in this direction would provide valuable insights in the field.

Acknowledgements HSD thanks UGC India for fellowship. This work was financially supported by Science and Engineering Research Board (SERB), Department of Science and Technology, India (Grant No. CRG/2022/007119); and Council of Scientific and Industrial Research (CSIR), Ministry of Science and Technology, India (Project No. 01 (3039)/21/EMR-II) awarded to HKK.

References

1. Winter M, Barnett B, Xu K (2018) Before li ion batteries. Chem Rev 118:11433–11456
2. Kim T, Song W, Son D-Y, Ono LK, Qi Y (2019) Lithium-ion batteries: outlook on present, future, and hybridized technologies. J Mater Chem A 7:2942–2964
3. Goodenough JB, Park K-S (2013) The li-ion rechargeable battery: a perspective. J Am Chem Soc 135:1167–1176
4. Goodenough JB, Kim Y (2010) Challenges for rechargeable li batteries. Chem Mater 22:587–603
5. Peled E, Menkin S (2017) Review-sei: past, present and future. J Electrochem Soc 164:A1703
6. Armand M, Tarascon J-M (2008) Building better batteries. Nature 451:652–657
7. Watanabe M, Thomas ML, Zhang S, Ueno K, Yasuda T, Dokko K (2017) Application of ionic liquids to energy storage and conversion materials and devices. Chem Rev 117:7190–7239
8. Matsumoto H (2014) Review: ionic liquids as a potential electrolyte for energy devices. In: 2014 IEEE International Nanoelectronics Conference (INEC), pp 1–4

9. Suo L, Borodin O, Gao T, Olguin M, Ho J, Fan X, Luo C, Wang C, Xu K (2015) "water-in-salt" electrolyte enables high-voltage aqueous lithium-ion chemistries. Science 350:938
10. Welton T (1999) Room-temperature ionic liquids solvents for synthesis and catalysis. Chem Rev 99:2071–2084
11. Lei Z, Chen B, Koo Y-M, MacFarlane DR (2017) Introduction: ionic liquids. Chem Rev 117(10):6633–6635
12. Seddon KR (2003) A taste of the future. Nat Mater 2:363
13. Davis JH Jr (2004) Task-specific ionic liquids. Chem Lett 33:1072–1077
14. Simon P, Gogotsi Y (2008) Materials for electrochemical capacitors. Nat Mater 7:845
15. Armand M, Endres F, MacFarlane DR, Ohno H, Scrosati B (2009) Ionic-liquid materials for the electrochemical challenges of the future. Nat Mater 8:621
16. Lu W, Fadeev AG, Qi B, Smela E, Mattes BR, Ding J, Spinks GM, Mazurkiewicz J, Zhou D, Wallace GG, MacFarlane DR, Forsyth SA, Forsyth M (2002) Use of ionic liquids for pi-conjugated polymer electrochemical devices. Science 297:983
17. MacFarlane DR, Forsyth M, Howlett PC, Pringle JM, Sun J, Annat G, Neil W, Izgorodina EI (2007) Ionic liquids in electrochemical devices and processes: managing interfacial electrochemistry. Acc Chem Res 40:1165–1173
18. Smiglak M, Metlen A, Rogers RD (2007) The second evolution of ionic liquids: From solvents and separations to advanced materials-energetic examples from the ionic liquid cookbook. Acc Chem Res 40:1182–1192
19. Greaves TL, Kennedy DF, Mudie ST, Drummond CJ (2010) Diversity observed in the nanostructure of protic ionic liquids. J Phys Chem B 114:10022–10031
20. Zein El Abedin S, Endres F (2007) Ionic liquids: The link to high-temperature molten salts? Acc Chem Res 40:1106–1113
21. Balducci A, Dugas R, Taberna PL, Simon P, Plée D, Mastragostino M, Passerini S (2007) High temperature carbon-carbon supercapacitor using ionic liquid as electrolyte. J Power Sources 165:922–927
22. Kim TY, Lee HW, Stoller M, Dreyer DR, Bielawski CW, Ruoff RS, Suh KS (2011) High-performance supercapacitors based on poly(ionic liquid)-modified graphene electrodes. ACS Nano 5:436–442
23. Lin R, Taberna P-L, Fantini S, Presser V, Pérez CR, Malbosc F, Rupesinghe NL, Teo KBK, Gogotsi Y, Simon P (2011) Capacitive energy storage from −50 to 100°c using an ionic liquid electrolyte. J Phys Chem Lett 2:2396–2401
24. Choi BG, Yang M, Jung SC, Lee KG, Kim J-G, Park H, Park TJ, Lee SB, Han Y-K, Huh YS (2013) Enhanced pseudocapacitance of ionic liquid/cobalt hydroxide nanohybrids. ACS Nano 7:2453–2460
25. Brandt A, Pohlmann S, Varzi A, Balducci A, Passerini S (2013) Ionic liquids in supercapacitors. MRS Bull 38:554–559
26. Wang H, Xu Z, Kohandehghan A, Li Z, Cui K, Tan X, Stephenson TJ, King'ondu CK, Holt CMB, Olsen BC, Tak JK, Harfield D, Anyia AO, Mitlin D (2013) Interconnected carbon nanosheets derived from hemp for ultrafast supercapacitors with high energy. ACS Nano 7:5131–5141
27. Suo L, Hu Y-S, Li H, Armand M, Chen L (2013) A new class of solvent-in-salt electrolyte for high-energy rechargeable metallic lithium batteries. Nature Commun 4:1481
28. Wang J, Yamada Y, Sodeyama K, Chiang CH, Tateyama Y, Yamada A (2016) Superconcentrated electrolytes for a high-voltage lithium-ion battery. Nature Commun 7:12032
29. Yamada Y, Usui K, Sodeyama K, Ko S, Tateyama Y, Yamada A (2016) Hydrate-melt electrolytes for high-energy-density aqueous batteries. Nat Energy 1:16129
30. Yamada Y, Yaegashi M, Abe T, Yamada A (2013) A superconcentrated ether electrolyte for fast-charging li-ion batteries. Chem Commun 49:11194–11196
31. Suo L, Borodin O, Sun W, Fan X, Yang C, Wang F, Gao T, Ma Z, Schroeder M, von Cresce A, Russell SM, Armand M, Angell A, Xu K, Wang C (2016) Advanced high-voltage aqueous lithium-ion battery enabled by "water-in-bisalt" electrolyte. Angew Chem Int Ed 55:7136–7141

32. Yamada Y, Yamada A (2015) Review-superconcentrated electrolytes for lithium batteries. J Electrochem Soc 162(14):A2406–A2423
33. Yang C, Chen J, Qing T, Fan X, Sun W, von Cresce A, Ding MS, Borodin O, Vatamanu J, Schroeder MA, Eidson N, Wang C, Xu K (2017) 4.0 v aqueous li-ion batteries. Joule 1:122–132
34. Kühnel R-S, Reber D, Battaglia C (2020) Perspective-electrochemical stability of water-in-salt electrolytes. J Electrochem Soc 167:070544
35. Yamada Y, Furukawa K, Sodeyama K, Kikuchi K, Yaegashi M, Tateyama Y, Yamada A (2014) Unusual stability of acetonitrile-based superconcentrated electrolytes for fast-charging lithium-ion batteries. J Am Chem Soc 136:5039–5046
36. Okuoka S-I, Ogasawara Y, Suga Y, Hibino M, Kudo T, Ono H, Yonehara K, Sumida Y, Yamada Y, Yamada A, Oshima M, Tochigi E, Shibata N, Ikuhara Y, Mizuno N (2014) A new sealed lithium-peroxide battery with a co-doped li2o cathode in a superconcentrated lithium bis(fluorosulfonyl)amide electrolyte. Sci Rep 4:5684
37. Dokko K, Watanabe D, Ugata Y, Thomas ML, Tsuzuki S, Shinoda W, Hashimoto K, Ueno K, Umebayashi Y, Watanabe M (2018) Direct evidence for li ion hopping conduction in highly concentrated sulfolane-based liquid electrolytes. J Phys Chem B 122:10736–10745
38. Qian J, Henderson WA, Xu W, Bhattacharya P, Engelhard M, Borodin O, Zhang J-G (2015) High rate and stable cycling of lithium metal anode. Nat Commun 6:6362
39. Yang J, Ding Y, Lian C, Ying S, Liu H (2020) Theoretical insights into the structures and capacitive performances of confined ionic liquids. Polymers 12(3):722
40. Herrera C, García G, Atilhan M, Aparicio S (2015) Nanowetting of graphene by ionic liquid droplets. J Phys Chem C 119(43):24529–24537
41. Burt R, Birkett G, Salanne M, Zhao XS (2016) Molecular dynamics simulations of the influence of drop size and surface potential on the contact angle of ionic-liquid droplets. J Phys Chem C 120(28):15244–15250
42. Li H, Sedev R, Ralston J (2011) Dynamic wetting of a fluoropolymer surface by ionic liquids. Phys Chem Chem Phys 13(9):3952–3959
43. Taherian F, Leroy F, Heim L-O, Bonaccurso E, van der Vegt NFA (2016) Mechanism for asymmetric nanoscale electrowetting of an ionic liquid on graphene. Langmuir 32(1):140–150
44. Malali S, Foroutan M (2017) Study of wetting behavior of bmim+/pf6- ionic liquid on tio2 (110) surface by molecular dynamics simulation. J Phys Chem C 121(21):11226–11233
45. Dong D, Vatamanu JP, Wei X, Bedrov D (2018) The 1-ethyl-3-methylimidazolium bis(trifluoromethylsulfonyl)-imide ionic liquid nanodroplets on solid surfaces and in electric field: a molecular dynamics simulation study. J Chem Phys 148:193833
46. Bordes E, Douce L, Quitevis EL, Padua AAH, Costa Gomes M (2018) Ionic liquids at the surface of graphite: wettability and structure. J Chem Phys 148:193840
47. Liu Z, Cui T, Li G, Endres F (2017) Interfacial nanostructure and asymmetric electrowetting of ionic liquids. Langmuir 33(38):9539–9547
48. Dhattarwal HS, Kashyap HK (2019) Molecular dynamics investigation of wetting-dewetting behavior of model carbon material by 1-butyl-3-methylimidazolium acetate ionic liquid nanodroplet. J Chem Phys 151:244705
49. Wang S, Li S, Cao Z, Yan T (2010) Molecular dynamic simulations of ionic liquids at graphite surface. J Phys Chem C 114:990–995
50. Feng G, Jiang X, Qiao R, Kornyshev AA (2014) Water in ionic liquids at electrified interfaces: the anatomy of electrosorption. ACS Nano 8:11685–11694
51. Sharma S, Kashyap HK (2015) Structure of quaternary ammonium ionic liquids at interfaces: effects of cation tail modification with isoelectronic groups. J Phys Chem C 119:23955–23967
52. Sharma S, Kashyap HK (2017) Interfacial structure of pyrrolidinium cation based ionic liquids at charged carbon electrodes: the role of linear and nonlinear alkyl tails. J Phys Chem C 121:13202–13210
53. Sharma S, Dhattarwal HS, Kashyap HK (2019) Molecular dynamics investigation of electrostatic properties of pyrrolidinium cation based ionic liquids near electrified carbon electrodes. J Mol Liq 291:111269

54. Gupta A, Dhattarwal HS, Kashyap HK (2021) Structure of cholinium glycinate biocompatible ionic liquid at graphite electrode interface. J Chem Phys 154:184702
55. Vatamanu J, Borodin O (2017) Ramifications of water-in-salt interfacial structure at charged electrodes for electrolyte electrochemical stability. J Phys Chem Lett 8:4362–4367
56. Li Z, Jeanmairet G, Méndez-Morales T, Rotenberg B, Salanne M (2018) Capacitive performance of water-in-salt electrolytes in supercapacitors: a simulation study. J Phys Chem C 122:23917–23924
57. McEldrew M, Goodwin ZAH, Kornyshev AA, Bazant MZ (2018) Theory of the double layer in water-in-salt electrolytes. J Phys Chem Lett 9:5840–5846
58. Ye J, Baumgaertel AC, Wang YM, Biener J, Biener MM (2015) Structural optimization of 3d porous electrodes for high-rate performance lithium ion batteries. ACS Nano 9:2194–2202
59. Vatamanu J, Vatamanu M, Borodin O, Bedrov D (2016) A comparative study of room temperature ionic liquids and their organic solvent mixtures near charged electrodes. J Phys: Condens Matter 28:464002
60. Vatamanu J, Bedrov D, Borodin O (2017) On the application of constant electrode potential simulation techniques in atomistic modelling of electric double layers. null 43:838–849
61. Zhang L, Wang H (2020) Anion intercalation into a graphite electrode from trimethyl phosphate. ACS Appl Mater Interfaces 12:47647–47654
62. Huang X, Margulis CJ, Berne BJ (2003) Dewetting-induced collapse of hydrophobic particles. Proc Natl Acad Sci 100:11953
63. Xu L, Molinero V (2010) Liquid-vapor oscillations of water nanoconfined between hydrophobic disks: thermodynamics and kinetics. J Phys Chem B 114:7320–7328
64. Remsing RC, Xi E, Vembanur S, Sharma S, Debenedetti PG, Garde S, Patel AJ (2015) Pathways to dewetting in hydrophobic confinement. Proc Natl Acad Sci 112(27):8181–8186
65. Altabet YE, Haji-Akbari A, Debenedetti PG (2017) Effect of material flexibility on the thermodynamics and kinetics of hydrophobically induced evaporation of water. Proc Natl Acad Sci 114(13):E2548–E2555
66. Cerdeiriña CA, Debenedetti PG, Rossky PJ, Giovambattista N (2011) Evaporation length scales of confined water and some common organic liquids. J Phys Chem Lett 2:1000–1003
67. Davoodabadi A, Ghasemi H (2021) Evaporation in nano/molecular materials. Adv Colloid Interface Sci 290:102385
68. Massé RC, Liu C, Li Y, Mai L, Cao G (2017) Energy storage through intercalation reactions: electrodes for rechargeable batteries. Natl Sci Rev 4:26–53
69. Zhu D, Fan H, Wang H (2021) Pf6- intercalation into graphite electrode from propylene carbonate. ACS Appl Energy Mater 4:2181–2189
70. Kondo Y, Miyahara Y, Fukutsuka T, Miyazaki K, Abe T (2019) Electrochemical intercalation of bis(fluorosulfonyl)amide anions into graphite from aqueous solutions. Electrochem Commun 100:26–29
71. Xia J, Wang J, Chao D, Chen Z, Liu Z, Kuo J-L, Yan J, Shen ZX (2017) Phase evolution of lithium intercalation dynamics in 2h-mos2. Nanoscale 9(22):7533–7540
72. Abbas G, Sonia FJ, Zafar ZA, Knížek K, Houdková J, Jiříček P, Bouša M, Plšek J, Kalbáč M, Červenka J, Frank O (2022) Influence of structural properties on (de-)intercalation of clo4- anion in graphite from concentrated aqueous electrolyte. Carbon 186:612–623
73. Rothermel S, Meister P, Schmuelling G, Fromm O, Meyer H-W, Nowak S, Winter M, Placke T (2014) Dual-graphite cells based on the reversible intercalation of bis(trifluoromethanesulfonyl)imide anions from an ionic liquid electrolyte. Energy Environ Sci 7(10):3412–3423
74. Shrivastav G, Remsing RC, Kashyap HK (2018) Capillary evaporation of the ionic liquid [EMIM][BF4] in nanoscale solvophobic confinement. J Chem Phys 148(19):193810
75. Dhattarwal HS, Remsing RC, Kashyap HK (2020) How flexibility of the nanoscale solvophobic confining material promotes capillary evaporation of ionic liquids. J Phys Chem C 124:4899–4906
76. Dhattarwal HS, Remsing RC, Kashyap HK (2021) Intercalation-deintercalation of water-in-salt electrolytes in nanoscale hydrophobic confinement. Nanoscale 13(7):4195–4205

77. Altabet YE, Debenedetti PG (2017) Communication: relationship between local structure and the stability of water in hydrophobic confinement. J Chem Phys 147:241102
78. Patel AJ, Varilly P, Chandler D (2010) Fluctuations of water near extended hydrophobic and hydrophilic surfaces. J Phys Chem B 114:1632–1637
79. Patel AJ, Varilly P, Chandler D, Garde S (2011) Quantifying density fluctuations in volumes of all shapes and sizes using indirect umbrella sampling. J Stat Phys 145:265–275
80. Kumar S, Rosenberg JM, Bouzida D, Swendsen RH, Kollman PA (1992) The weighted histogram analysis method for free-energy calculations on biomolecules. i. the method. J Comput Chem 13:1011–1021
81. Altabet YE, Debenedetti PG (2014) The role of material flexibility on the drying transition of water between hydrophobic objects: a thermodynamic analysis. J Chem Phys 141:18C531
82. Alibalazadeh M, Foroutan M (2015) Specific distributions of anions and cations of an ionic liquid through confinement between graphene sheets. J Mol Model 21:168